

# Self-organized intermittent plastic flow in bulk metallic glasses

G. Wang<sup>a</sup>, K.C. Chan<sup>a,\*</sup>, L. Xia<sup>a</sup>, P. Yu<sup>a</sup>, J. Shen<sup>b</sup>, W.H. Wang<sup>c</sup>

<sup>a</sup> *Advanced Manufacturing Technology Research Centre, Department of Industrial and Systems Engineering, Hong Kong Polytechnic University, Kowloon, Hong Kong, China*

<sup>b</sup> *School of Materials Science and Engineering, Harbin Institute of Technology, Harbin 150001, China*

<sup>c</sup> *Institute of Physics, Chinese Academy of Sciences, Beijing 100080, China*

Received 22 June 2009; received in revised form 17 August 2009; accepted 18 August 2009

Available online 16 September 2009

## Abstract

Under stress, bulk metallic glasses irreversibly deform through shear banding processes that manifest as serrated flow behavior. These serration events exhibit a shock-and-aftershock, earthquake-like behavior. Statistical analysis shows that the shear avalanches can self-organize to a critical state (SOC). In analogy to the smooth macroscopic-scale crystalline plasticity that arises from the spatio-temporal averages of disruptive earthquake-like events at the nanometer scale, shear avalanches in glassy metals are another model system that can be used to study SOC behavior. With our understanding of SOC behavior, we further demonstrate how to enhance the plasticity of glassy (brittle) materials. It is expected that the findings can be extended to other glassy or brittle materials.

© 2009 Acta Materialia Inc. Published by Elsevier Ltd. All rights reserved.

**Keywords:** Intermittent avalanche; Self-organized critical behavior; Plastic deformation; Bulk metallic glasses

## 1. Introduction

The deformation of crystalline metals has been a topic of extensive research for many years and there are different approaches or models established to describe the deformation [1]. Although the continuum approach can perfectly elucidate some deformation phenomena, such as strain hardening, yielding and plastic flow, it fails to account for microscopic plastic deformation because of discontinuous defect motions in crystalline materials, such as microfracture process and avalanches in the motion of dislocations [2]. In recent years, with the aim of gaining a better understanding of the microscopic inhomogeneous deformation behavior of crystalline metals, statistical deformation analysis has been conducted [3–6]. In stressed ice single crystals, a self-organization of collective dislocation dynamics into a scale-free pattern of dislocation avalanches is characterized by intermittency, power-law distributions of avalanche sizes,

complex spatio-temporal correlations and aftershock triggering [3]. Polycrystalline plasticity is also characterized by intermittency and dislocation avalanches, but, due to hindrance by grain boundaries, internal stresses will eventually push the dynamical system into a supercritical state, off the scale-invariant critical regime, and then trigger secondary avalanches in neighboring grains [4]. This scale-free intermittent flow behavior is also observed in microcrystals, where it is dependent on the microcrystal size [5,6]. As the microcrystal size decreases to zero, i.e. a glassy state, it is unclear whether the plastic flow follows this scale-free intermittent behavior.

The development of bulk metallic glasses (BMGs) exhibiting different compressive ductilities provides a good model for facilitating the statistic analysis of the plastic flow of glassy materials [7–11]. As this kind of material contains no defects to control the mechanical behavior, the formation and propagation of shear bands replace the dislocation motion to produce plastic strain [12,13]. This shear banding behavior in BMGs is manifested as a sequence of serration events (serrated flow), including the aggregation and release of deformation energy during compressive plastic

\* Corresponding author. Tel.: +852 27664981; fax: +852 23625267.

E-mail address: [mfkchan@polyu.edu.hk](mailto:mfkchan@polyu.edu.hk) (K.C. Chan).

deformation, which feature as discrete bursts of plasticity [14]. The shear avalanche then results in the catastrophic fracture of BMGs. Although it is of the utmost importance to understand the dynamic intermittent shear motion of BMGs so as to improve their ductility, the reason for their intermittent serrated flow behavior is still not very clear, and the correlation between the dynamics of the intermittent strain bursts and the macroscopic plastic instability of BMGs has yet to be reported. In this paper, statistical deformation analysis is conducted for five BMGs with different plasticity (i.e.  $Zr_{55}Cu_{30}Al_{10}Ni_5$ ,  $Zr_{41.25}Ti_{13.75}Ni_{10}Cu_{12.5}Be_{22.5}$ ,  $Cu_{42.5}Ti_{42.5}Zr_{2.5}Hf_5Ni_{7.5}$ ,  $Zr_{51}Cu_{23.25}Ni_{13.5}Al_{12.25}$  and  $Cu_{47.5}Zr_{47.5}Al_5$  BMGs), and the relationships between ductility and the possible cumulative distribution of shear avalanches is characterized.

## 2. Experimental procedures

Alloy ingots were prepared by arc melting a mixture of pure metal elements in an argon atmosphere, followed by suction casting into copper moulds to form rod-like BMG samples 2 mm in diameter. The structure of the glassy phase of the as-cast BMG specimens was checked by transmission electron microscopy and X-ray diffraction, and the surface of the specimens was observed with a JEOL JSM-6335F scanning electron microscope (SEM). Two ends of compressive test specimens with a length/diameter ratio of 2 were carefully ground to 1  $\mu$ m. Compression tes-

tes were conducted in a servo-hydraulic driving MTS-type machine with a strain rate of  $2.5 \times 10^{-4} s^{-1}$ .

A nickel layer was electrodeposited on the surface of the  $Zr_{41.25}Ti_{13.75}Ni_{10}Cu_{12.5}Be_{22.5}$  BMG in an aqueous nickel sulfamate–chloride electrolyte. A nickel plate with a purity of 99.99% was used as an anode and the BMG rod was used as a cathode. The BMG rod was rotated driven by a motor at a rotate speed of 60 rpm to guarantee that the electrodeposited nickel sleeve had an even thickness. Different plating times (1 and 3 h) were used to make Ni sleeves of different thicknesses. Electrodeposition was conducted at a temperature of 25 °C, with a current of 40 mA and a voltage of 1.1 V. The distance between the anode and the cathode was 30 mm.

## 3. Self-organization to a critical state (SOC) behavior in the serrated flow of BMGs

The compressive nominal stress–strain ( $\sigma$ – $\epsilon$ ) curves of the five as-cast BMGs exhibit serrated flow behavior after yielding (see Fig. 1a). The mechanical property parameters are listed in Table 1. The serration process is characterized by repeating cycles of a sudden stress drop followed by reloading elastically (see Fig. 1b), and exhibits the following characteristics. First, the stress–time ( $\sigma$ – $t$ ) curve and the corresponding  $|d\sigma/dt|$  plot for the plastic strain stage clearly show that the time interval ( $t_n$ ) between any two neighboring serrations is inhomogeneous, i.e.  $t_0 \neq t_1 \neq \dots \neq t_{n+1}$ , which

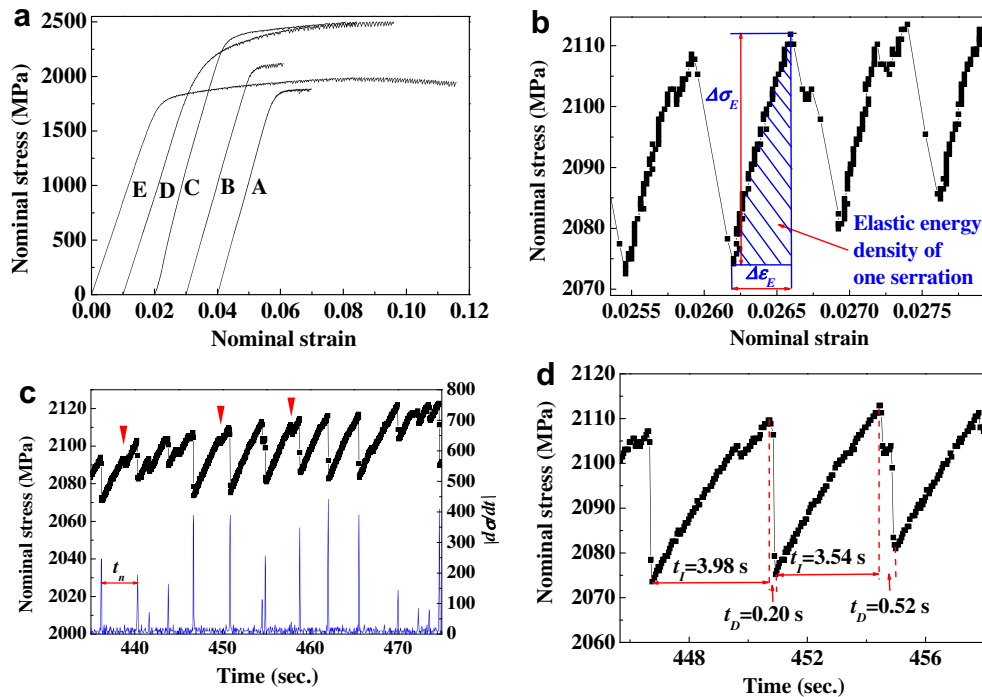


Fig. 1. Serrated flow behavior in the compressive deformation of BMGs. (a) Compressive nominal stress–strain curves of five BMGs. Curve A:  $Zr_{55}Cu_{30}Al_{10}Ni_5$ ; Curve B:  $Zr_{41.25}Ti_{13.75}Ni_{10}Cu_{12.5}Be_{22.5}$ ; Curve C:  $Cu_{42.5}Ti_{42.5}Zr_{2.5}Hf_5Ni_{7.5}$ ; Curve D:  $Zr_{51}Cu_{23.25}Ni_{13.5}Al_{12.25}$  and Curve E:  $Cu_{47.5}Zr_{47.5}Al_5$ . (b) Elastic energy density for one serration event. The serration is extracted from Curve B. (c) Stress–time curve and its corresponding plot of  $|d\sigma/dt|$  for a part of serrations in Curve B. (d) Stress–time curve for two representative serrations in Curve B.  $t_I$  is the stress increase time and  $t_D$  is the stress drop time.

Table 1  
Plastic strains ( $\varepsilon_p$ ), Young's moduli ( $E$ ), yield stresses ( $\sigma_E$ ), scaling exponents ( $\beta$ ), normalization constants ( $A$ ) and cut-offs for the elastic energy density ( $\delta_C$ ) of the BMGs.

BMGs	$\varepsilon_F$	$\varepsilon_p$	$E$ (GPa)	$\sigma_E$ (MPa)	$\beta$	$\delta_C$ (J m <sup>-3</sup> )	$A$
Zr <sub>55</sub> Cu <sub>30</sub> Al <sub>10</sub> Ni <sub>5</sub>	0.030	0.014	104	1677	0.40	2950	11.4
Zr <sub>41.25</sub> Ti <sub>13.75</sub> Ni <sub>10</sub> Cu <sub>12.5</sub> Be <sub>22.5</sub>	0.031	0.012	101	1925	0.39	4804	9.1
Cu <sub>42.5</sub> Ti <sub>42.5</sub> Zr <sub>2.5</sub> Hf <sub>5</sub> Ni <sub>7.5</sub>	0.064	0.044	107	2096	0.41	5768	9.9
Zr <sub>51</sub> Cu <sub>23.25</sub> Ni <sub>13.5</sub> Al <sub>12.25</sub>	0.086	0.066	90	1805	0.39	6649	8.8
Cu <sub>47.5</sub> Zr <sub>47.5</sub> Al <sub>5</sub>	0.116	0.096	83	1638	0.40	12635	9.5
17.8 $\mu$ m thick Ni sleeve	0.046	0.028	91	1644	0.28	3485	4.3
55.3 $\mu$ m thick Ni sleeve	0.111	0.089	81	1770	0.29	2820	3.8

suggests that the serration events lack any typical time scale (see Fig. 1c) [2]. Secondly, the stress increase time ( $t_I$ ) being 7–21 times larger than the stress drop time ( $t_D$ ) (see Fig. 1d) suggests that the process under external stress (stress increase) is much slower than the internal relaxation process (stress drop). Thirdly, because the number of serration events ranged from 33 to 204 in different BMGs and one serration event could correspond to the operation of several shear bands [10], the serrated flow include many shear bands, i.e. a large number of interacting entities. These characteristics indicate that the plastic deformation of BMGs should be considered within a close-to-criticality nonequilibrium framework [13], reminiscent of the concept of SOC behavior [15]. In addition to the three characteristics mentioned above, the conditions necessary for SOC behavior include statistical properties following a power-law distribution, which will be discussed next.

The stress–time curve (see Fig. 1c) shows that some tiny stress undulations (indicated by triangles) appear on the serration events. These small stress undulations are possibly induced by a vibration resulting from the motion of the cross-heads in the MTS machine. In Fig. 2, the compression stress–strain curve of the Cu<sub>47.5</sub>Zr<sub>47.5</sub>Al<sub>5</sub> BMG (curve E in Fig. 1a) is chosen as an example to show how the influence of the vibration from the MTS machine is eliminated. Theoretically, the elastic deformation of BMGs must exhibit a perfect linear behavior. However, by enlarging the stress–strain curve in the elastic deformation stage (enclosed in a rectangle in Fig. 2a), small strain fluctuations (shown in the inset of Fig. 2a) can be easily seen, which is possibly generated by the vibration of the MTS machine. Through linear fitting in the elastic deformation stage, a baseline (or an ideal linear elastic stress–strain curve) is plotted in Fig. 2b. When the baseline is subtracted from

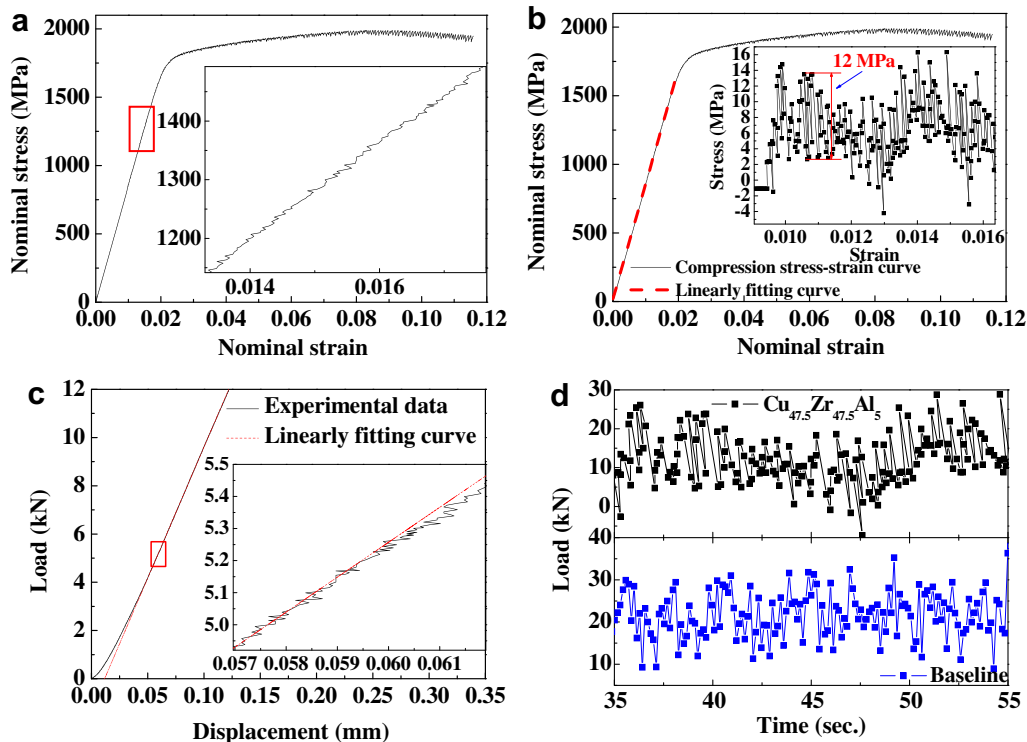


Fig. 2. Sketch of the method for eliminating the influence from the vibration of the MTS machine. (a) Strain fluctuation in elastic deformation stage. (b) Calculation of the stress vibration amplitude. (c) Compressive load–displacement curve of the MTS machine (baseline) without a sample. (d) Load–time curves of the baseline from the MTS machine and the BMG, respectively, after subtracting the linear fitting curves.

the actual stress–strain curve, the stress vibration amplitude of approximately of 12 MPa can be calculated, as shown in the inset of Fig. 2b. The stress fluctuation curve was also transformed to a load–time curve, as shown in Fig. 2d. In order to confirm that this vibration resulted from the natural vibration of the MTS machine, a compression test without BMG sample was conducted. The baseline vibration of the MTS machine, i.e. the load–displacement curve of the MTS machine without any sample, was obtained, and is plotted in Fig. 2c. Small displacement fluctuations were observed (shown in the inset of Fig. 2c) by enlarging the baseline enclosed by the rectangle. After subtracting the linearly fitting curve (see Fig. 2c), the load–time curve of the baseline was found to match the load–time curve of the  $\text{Cu}_{47.5}\text{Zr}_{47.5}\text{Al}_5$  BMG very well (see Fig. 2d), illustrating that the vibration in the elastic deformation was caused by the MTS machine. In order to eliminate this effect, any serration events with a stress increase less than 12 MPa in the plastic strain stage were excluded in our statistical analysis. Similarly, the stress vibration amplitudes for other four BMGs were found to range from 9 to 12 MPa (not shown).

One serration event includes a process of elastic energy accumulation and a process of elastic energy release. The elastic energy density of one serration event ( $\Delta\delta$ ) is  $\Delta\delta = \frac{1}{2}\Delta\sigma_E\Delta\varepsilon_E$ , where  $\Delta\sigma_E$  and  $\Delta\varepsilon_E$  are the elastic stress and elastic strain in one serration event, respectively (see Fig. 1b) [14]. Ergodic processing of the elastic energy density, as shown in Fig. 3, shows that a cumulative probability distribution, i.e. the percentage of the number of serration events with the elastic energy density being larger than an elastic energy density,  $P(\geq\Delta\delta)$ , is nonlinearly dependent on the value of  $\Delta\delta$  [16]. It is obvious that smaller elastic energy densities are more probable and will follow a power-law distribution. The larger elastic energy densities

do not follow a power-law distribution, and decrease exponentially in probability. The cumulative probability distributions of the five BMGs have a universal scaling function, which can be approximated well by a power-law distribution function accompanied with a squared exponential decay function [6,17]:

$$P(\geq\Delta\delta) = A\Delta\delta^{-\beta} \exp[-(\Delta\delta/\delta_C)^2] \quad (1)$$

where  $A$  is a normalization constant,  $\beta$  is a scaling exponent and  $\delta_C$  is the cut-off elastic energy density. The fitting parameters for the five BMGs are listed in Table 1. The  $\beta$  values are kept constant at  $0.40 \pm 0.01$ . Therefore, we have essentially a power-law relation with an exponent of about 0.40, up to the larger value of the elastic energy density, i.e. the  $\delta_C$  value, where the squared exponential decay factor comes into play. In contrast to the  $\beta$  value, which is constant, the  $\delta_C$  value increases with the increase in the ductility of the BMGs. Three parameters,  $\beta$ ,  $\Delta\delta$  and  $\delta_C$ , provide a fingerprint reflecting the dynamics of shear deformation in BMGs.

As the release of elastic energy mainly activates flow events in liquid-like solids [18,19] and the flow events in glassy metals are thought to be shear transformation zones (STZs) [20–23], the elastic energy of serration events is consumed by the STZs configurationally hopping. The activation barrier ( $W$ ) for one STZ configurationally hopping between two stable states can be expressed as  $W = W_g(G/G_g)^2$ , where  $W_g$  and  $G_g$  are the flow barrier and shear modulus, respectively, at the glass transition temperature, and  $G$  is the shear modulus at room temperature [24]. For most metallic glasses, the values of  $W_g$  and  $G_g$  are  $\sim 2.5 \times 10^{-19}$  J and  $\sim 30$  GPa, respectively [24,25]. The value of  $G$  is 34.8 GPa ( $\text{Zr}_{51}\text{Cu}_{23.25}\text{Ni}_{13.5}\text{Al}_{12.25}$  BMG), measured ultrasonically. The activation barrier for one STZ can then be estimated to be approximately  $3.4 \times 10^{-19}$  J in BMGs. Since the elastic energy in the serration event is used to acti-

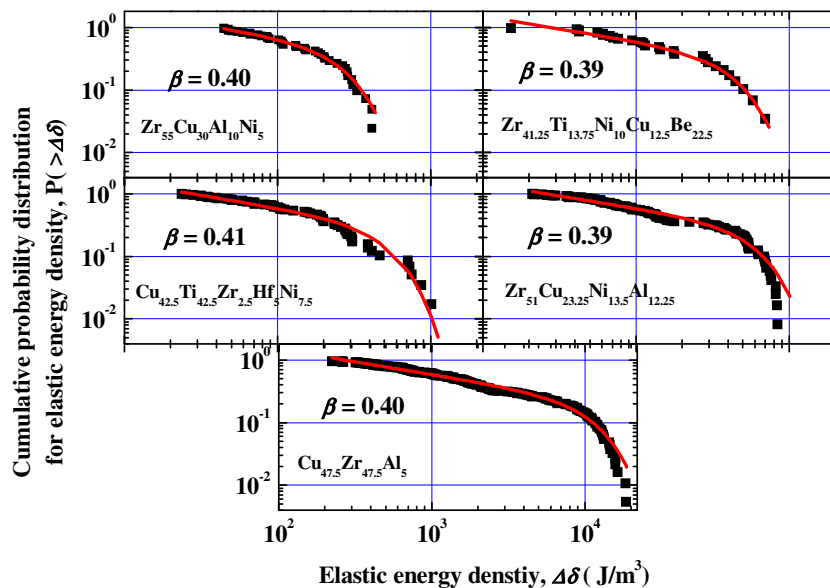


Fig. 3. Cumulative probability distributions for the elastic energy densities of the five BMGs. The scattering points are experimentally measured from the compressive stress–strain curves. The solid lines are fitted by Eq. (1).

vate the motion of the STZs, the amount of the hopped STZs in one serration event ( $N$ ) can be calculated by  $N = \Delta\delta/W$ . Multiplying the effective STZ volume ( $\Omega$ ), the amount of the hopped STZs can reflect a volume of shear band formed in one serration event. In the present study, since the shear band extends along a shear plane which deviates from the compression direction by  $42^\circ$ , the shear plane area ( $A$ ) is approximately  $4.7 \times 10^{-6} \text{ m}^2$ . The thickness of the shear band is assumed to be approximately 10 nm [26]. Then the volume of one shear band fully crossing the shear plane of the BMGs is calculated to be approximately  $4.7 \times 10^{13} \text{ nm}^3$ . Considering that the effective STZ volume roughly ranges from  $2.5$  to  $6.6 \text{ nm}^3$  [27], one shear band formation should be composed of  $7.1 \times 10^{12}$ – $1.9 \times 10^{13}$  hopped STZs, so it should take  $2.4 \times 10^{-6}$ – $6.5 \times 10^{-6} \text{ J}$  for a shear band to be fully sheared across the shear plane of the BMG samples. The corresponding energy density is approximately 190–513  $\text{J m}^{-3}$  due to our sample volume of  $\sim 12.6 \times 10^{-9} \text{ m}^3$ . The elastic energy densities in the serration events of the five BMGs ranged from 153 to 18553  $\text{J m}^{-3}$  (cf. Fig. 3).

It is obvious that the lowest elastic energy density of 153  $\text{J m}^{-3}$  measured from the compression stress–strain curves is lower than the range of the elastic energy density for the shear band formation (190–513  $\text{J m}^{-3}$ ), which suggests that, in the smaller serration events, the shear band possibly cannot shear across the whole cross-section of the specimen. To confirm this, we traced several shear bands on the  $\text{Zr}_{51}\text{Cu}_{23.25}\text{Ni}_{13.5}\text{Al}_{12.25}$  BMG strained to  $\sim 0.05$  by using the SEM (see Fig. 4a–c). Fig. 4b and c shows that highly branched secondary shear bands emanate from a primary shear band and that they are arrested and cannot sweep the whole shear plane. It is obvious that, besides the primary shear bands formation, the emanation of the branched secondary shear bands also consume a part of elastic energy. Considering this, even the serration events with a large elastic energy, i.e.  $>513 \text{ J m}^{-3}$ , cannot possibly provide sufficient energy to make the shear band shearing across the whole shear plane of the specimen.

For the larger serration events, i.e. those with elastic energy in the serrations  $\gg 513 \text{ J m}^{-3}$ , the experimental results suggest that the simultaneous formation of several shear bands and the shear displacing along a shear plane (see Fig. 4e) could consume the elastic energy [10]. In particular, for these larger serration events, the shear displacement needs more energy to activate more STZs in one serration event operation, which results in a higher elastic energy density (see Fig. 4e). Accompanying this shear displacement, a viscous layer will be formed in the shear bands due to adiabatic heating, which must consume a part of elastic energy [28]. Once the viscous layer has formed in the shear bands, the shear modulus will dramatically decrease, suggesting that the activation barrier of the STZ will be reduced due to  $W = (8/\pi^2)\gamma_c^2 G \Omega$  (where  $\gamma_c$  is the shear strain limit of BMGs [29]). As such, the elastic energy released from the serration events will mainly be consumed by adiabatic heating.

The necessary energy of adiabatic heating ( $\Gamma_A$ ) for one shear band shearing across whole cross-section of specimen

can be expressed as  $\Gamma_A = A l_t \rho C_p \Delta T$ , where  $A$  is the shear plane area ( $\sim 4.7 \times 10^{-6} \text{ m}^2$ ),  $\rho$  is the density ( $\sim 6.5 \times 10^6 \text{ g m}^{-3}$ ),  $l_t$  is the thickness of shear band (10 nm),  $C_p$  is the heat capacity and  $\Delta T$  is the adiabatic heating temperature [30]. In the present study, the  $\rho$  value is approximately  $6.5 \times 10^6 \text{ g m}^{-3}$ , the  $C_p$  value is  $\sim 1 \text{ J g}^{-1} \text{ K}^{-1}$  [31] and the  $\Delta T$  value is approximation 377 K according to experimental observations [32]. Thus the  $\Gamma_A$  value can be roughly estimated to be  $1.2 \times 10^{-4} \text{ J}$ , i.e. 9524  $\text{J m}^{-3}$ . Considering that the shear displacement possibly occurs in several shear bands, the actual  $\Gamma_A$  value must be higher than the estimated value of 9524  $\text{J m}^{-3}$ . Therefore, the estimated value is consistent with the experimental value of  $\sim 18,000 \text{ J m}^{-3}$ . This suggests that the elastic energy density,  $\Delta\delta$ , is associated with the shear avalanche size although it is not possible to quantitatively construct the link between the elastic energy of one serration event and shear banding.

Introducing the squared exponential decay function into the power-law function accounts for the finite elastic energy in the serration event [33]. The  $\delta_C$  value is a characteristic parameter that can be linked to a microstructural characteristic scale, such as the dislocation propagation characteristic length confined by the grain boundary in crystalline solids [13]. For the BMGs, since the  $\Delta\delta$  value is associated with the amount of the STZs moved, the  $\delta_C$  value should correspond to the characteristic shear size of the BMGs. Larger ductility indicates that more STZs will be triggered to render the shear deformation, which results in an increase in the characteristic shear size.

The universal exponent of 0.40 in different BMGs confirms that the serrated flow behavior is SOC behavior [6,16,34,35]. The serrated flow behavior of BMGs is similar to that of polycrystals and rock rupture [4,36], but differs from that of single crystals in two ways: (i) the observed power-law exponent is independent of plastic strain, yield stress, chemical composition, and so forth and (ii) the cut-off of this power-law scaling is observed towards large amplitudes. An important feature of SOC behavior is a self-similar or scale-free pattern, which means that structures on one scale appear to be the same as structures on other scales. To further characterize this SOC behavior, we looked further at the elastic energy density distribution along the strain of the five BMGs further observed (see Fig. 5).

The elastic energy distribution of the ductile BMGs ( $\text{Cu}_{42.5}\text{Ti}_{42.5}\text{Zr}_{2.5}\text{Hf}_{5}\text{Ni}_{7.5}$ ,  $\text{Zr}_{51}\text{Cu}_{23.25}\text{Ni}_{13.5}\text{Al}_{12.25}$  and  $\text{Cu}_{47.5}\text{Zr}_{47.5}\text{Al}_5$ ) can be divided into Region I and Region II (see Fig. 5). Serration events in Region II have greater elastic energy than those in Region I, which is shown in Fig. 5c–e. Among the BMGs with less ductility (see Fig. 5a and b), the two divided regions are not significant.

The enlarged stress–strain curve of the  $\text{Zr}_{51}\text{Cu}_{23.25}\text{Ni}_{13.5}\text{Al}_{12.25}$  BMG (representing the ductile BMGs) is shown in Fig. 6a. The profile of the stress–strain curve in Region I shows that a large serration event is frequently followed by a succession of serration events with a much smaller degree of elastic energy (Curve I in Fig. 6a). This

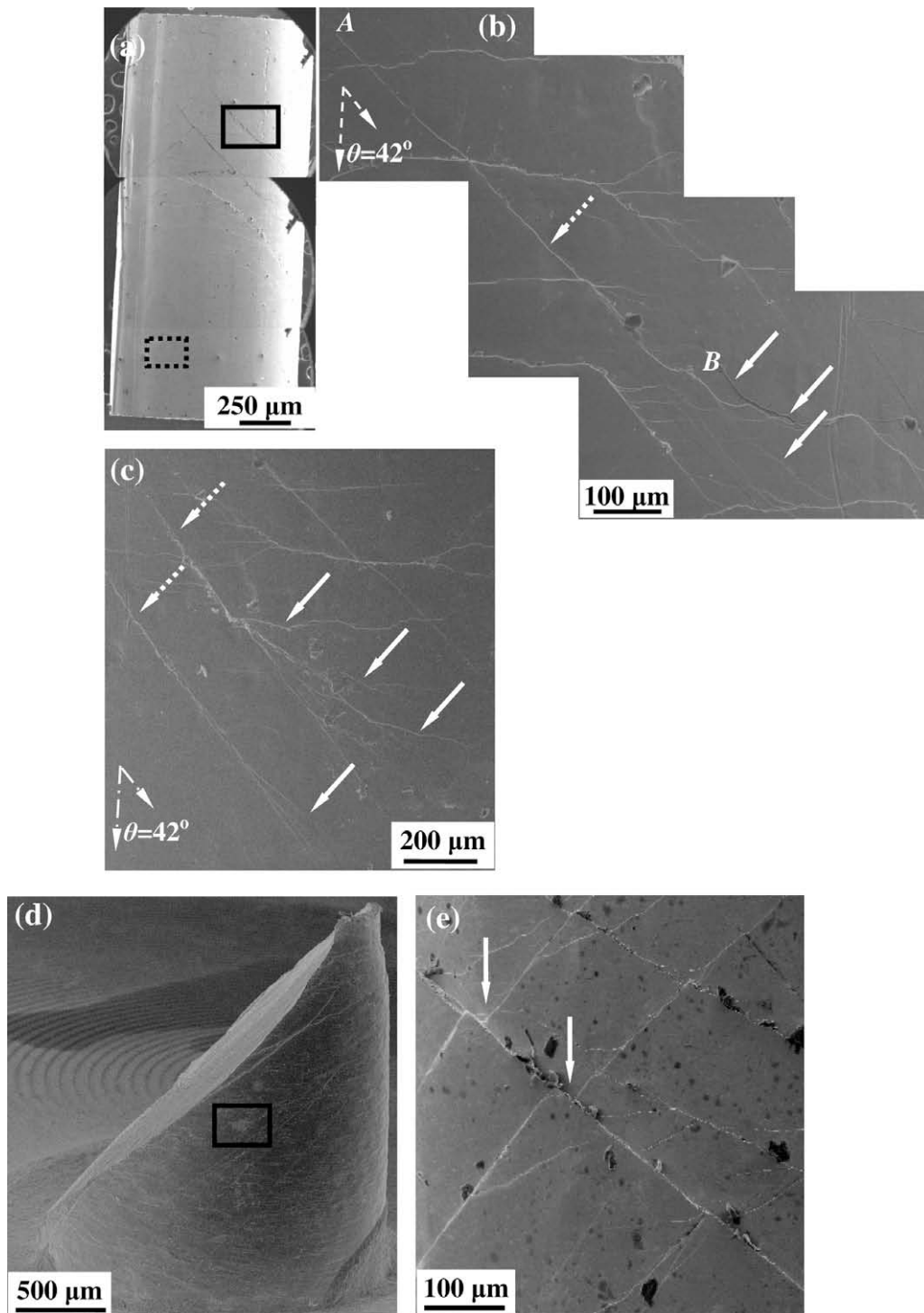


Fig. 4. SEM images for shear bands evolution on the surface of the  $Zr_{51}Cu_{23.25}Ni_{13.5}Al_{12.25}$  BMG. (a) Overview of the BMG strained to  $\sim 0.05$ . (b) The morphology corresponding to the area circled by a dot rectangle in (a) shows that one shear band does not shear across the whole cross-section of specimen (pointed out by a dot arrow). Points *A* and *B* are the shear band nucleation point and the branched point, respectively. The branched shear bands are indicated by solid arrows. (c) The morphology of the branched shear bands, corresponding to the area circled by a solid rectangle in (a). The main shear bands are indicated by dotted arrows and the branched shear bands are indicated by solid arrows. (d) Overview of the fractured BMG. (e) The shear displacement along one shear plane is indicated by arrows on the fractured BMG, corresponding to the area enclosed by a rectangle in (d).

behavior is analogous to that a stress shock under rising strain is followed by several aftershocks at smaller magnitudes. The smaller stress undulations in the aftershocks, i.e. the smaller serration events, can push the system to

self-organize to a new critical state. In Region II, the serration events are of greater magnitude and are not followed by smaller serration events, i.e. after the main shock, smaller aftershocks do not occur, which means that self-organi-

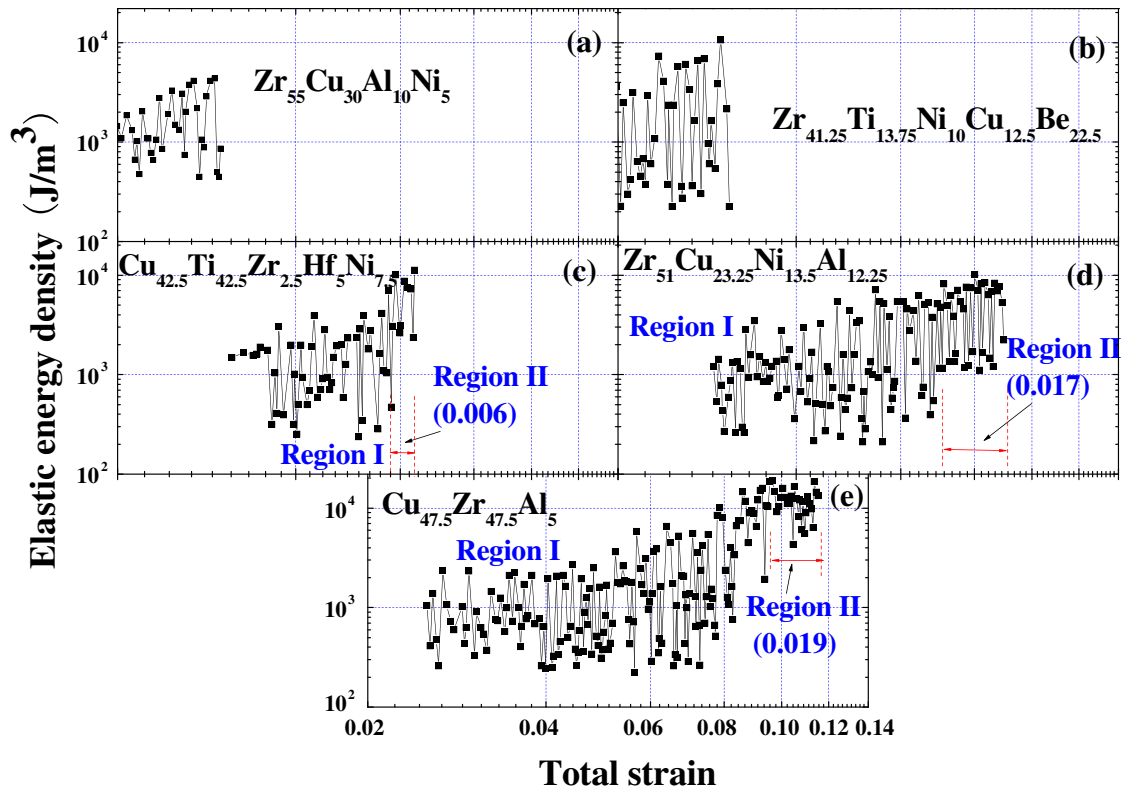


Fig. 5. Elastic energy density distribution spectra along the strains of the five BMGs. Arrow bars indicate the non-SOC regimes.

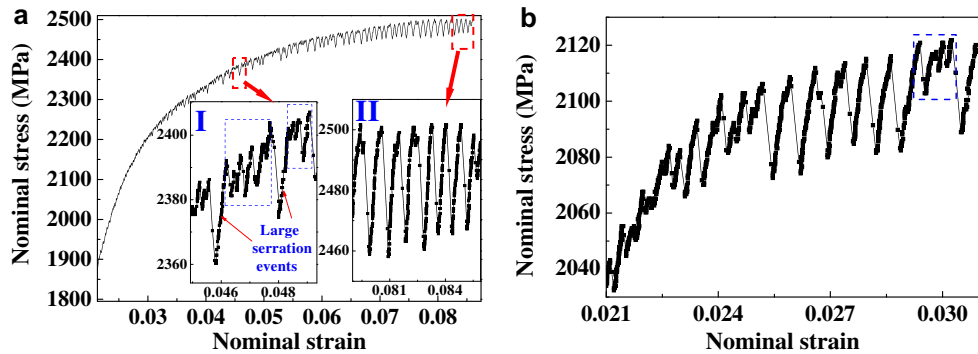


Fig. 6. Detail plastic stress–strain curves for the  $Zr_{51}Cu_{23.25}Ni_{13.5}Al_{12.25}$  and  $Zr_{41.25}Ti_{13.75}Ni_{10}Cu_{12.5}Be_{22.5}$  BMGs. (a) Stress–strain curve for the  $Zr_{51}Cu_{23.25}Ni_{13.5}Al_{12.25}$  BMG. Curves I and II indicate the small plastic strain regime and the fracture regime, respectively. The serration events with smaller elastic energy densities are covered by blue boxes. (b) Stress–strain curve for the  $Zr_{41.25}Ti_{13.75}Ni_{10}Cu_{12.5}Be_{22.5}$  BMG. The serration events with smaller elastic energy densities are covered by a blue box.

zation behavior is weaker (Curve II in Fig. 6a). Moreover, for the BMG with the least plasticity ( $Zr_{41.25}Ti_{13.75}Ni_{10}Cu_{12.5}Be_{22.5}$ ), although larger serration events followed by several smaller events could be observed (enclosed by a rectangle in Fig. 6b), the number is much less than that in the ductile BMGs, which suggests that SOC behavior is weak in the BMGs with smaller plasticity. On the other hand, the smaller  $\delta_C$  values in the two BMGs with the smallest plasticity suggest that the exponential decay happens in a smaller elastic energy magnitude and the STZs activated in whole serrated flow are much less than those in the ductile BMGs. In this case, there is not enough spatio-tempo-

ral medium to bear the self-organization process for the SOC behavior, thus a tiny plastic flow appears.

The self-similar pattern presenting in the serration events is reminiscent of the fractal network [37]. The fractal dimension given by  $D_f = 1/\beta = 2.49$  in the plastic strained BMGs, which is comparable to the fractal dimension of the structure in BMGs (which is 2.31) [37]. The structure of BMGs are characterized by efficiently packed clusters, usually well-defined as medium-range order (MRO) on a scale of approximately 1–2 nm, which is on the same length scale of STZs [27]. These packed MRO construct the fractal network [37]. Subjected to shear stress, these MROs (or

STZs) will be activated and moved to shape the serrated flow in the macroscope. It can thus be reasonably deduced that the dynamic behavior of serrated flow originates from the atomic structural fractal network of glassy phase because the similar fractal dimensions happen in the serrated flow and the packed MRO structure, respectively.

#### 4. Effect of the external disturbance on serrated flow

Based on the above discussion, we suppose that if shear avalanches in the serrated flow stage can self-organize to a

critical state, then the plasticity of BMGs will be improved. To confirm this conjecture, we investigated the serrated flow behavior of the  $Zr_{41.25}Ti_{13.75}Ni_{10}Cu_{12.5}Be_{22.5}$  BMG with different strain abilities. Enlightened by the case of geometric confinement enhancing the plasticity of BMGs [38], we electrodeposited a layer of nickel on the surface of the  $Zr_{41.25}Ti_{13.75}Ni_{10}Cu_{12.5}Be_{22.5}$  BMG. The Ni sleeve wraps perfectly around the BMG rod (see the insets in Fig. 7a and b), which suggests that lateral confinement during compressive deformation can effectively disturb the plastic deformation of the BMG. Increasing the thickness

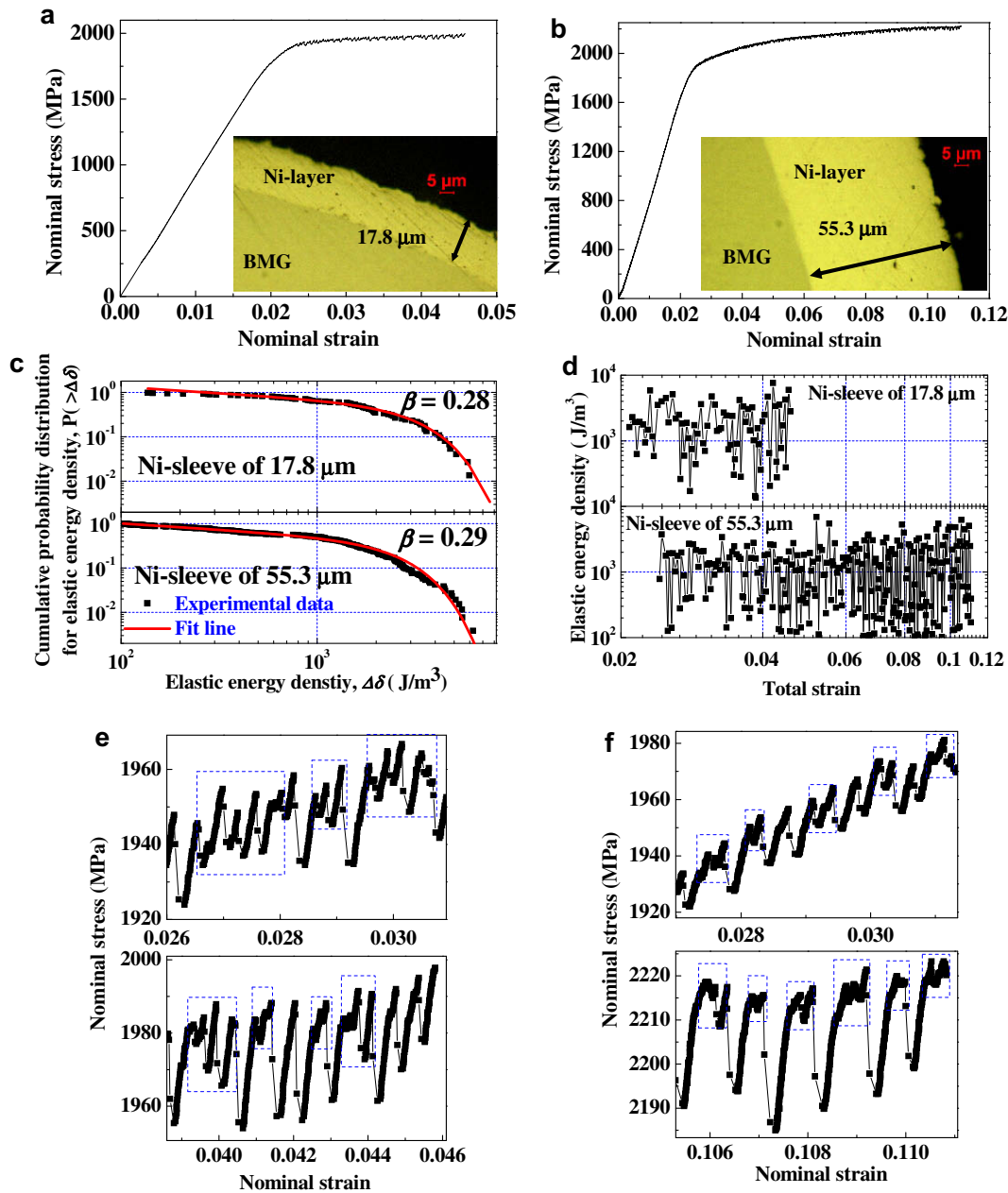


Fig. 7. (a and b) Compression nominal stress–strain curves of the  $Zr_{41.25}Ti_{13.75}Ni_{10}Cu_{12.5}Be_{22.5}$  BMGs coated with a 17.8 and 55.3  $\mu m$  thick Ni sleeve, respectively. (c) The cumulative probability distributions for the elastic energy densities. (d) The elastic energy density distribution spectra along the strains. (e) The plastic strain profile of the BMG coated with the 17.8  $\mu m$  thick Ni sleeve at two different strains. The serration events with smaller elastic energy densities are covered by blue boxes. (f) The plastic strain profile of the BMG coated with the 55.3  $\mu m$  thick Ni sleeve at two different strains. The serration events with smaller elastic energy densities are covered by blue boxes.

of the Ni sleeve can improve the plasticity of the BMG, as shown in Fig. 7a and b. The cumulative probability distributions of the elastic energy density of the BMGs with different Ni sleeve thicknesses also follow the power-law distribution function (see Fig. 7c). The  $\beta$  value and cut-off amplitudes of  $\delta_C$  are lower than those of the original  $Zr_{41.25}Ti_{13.75}Ni_{10}Cu_{12.5}Be_{22.5}$  BMG (Table 1). The plastic mechanism of the coated BMG includes shear banding and a dislocation motion resulting from the crystalline Ni sleeve, which results in the  $\beta$  value decreasing slightly compared to that in the original BMG [4]. Furthermore, because the yield strength of Ni film is as high as  $\sim 1050$  MPa [39] during the plastic strain, the Ni sleeve can provide a lateral confining stress that suppresses shear displacement in the radial direction. At the same, the Ni sleeve expands less than the BMG in the radial direction because the Poisson's ratio of nickel (0.30 [38]) is lower than that of the original BMG (0.36) [40], which further increases the confining pressure. This geometric confining pressure can lead to highly dense shear bands [38,41], which means that the plastic strain can be spread to more shear bands, thus reducing the shear avalanche size. This leads to decreases in the cut-off amplitudes of  $\delta_C$  and an increase in ductility. Compared with that in the original BMG, the elastic energy density distribution spectra do not show a significant Region II, i.e. a larger elastic energy density region, before fracturing (see Fig. 7d). Further enlargements of the stress-strain curves in Fig. 7a and b show the self-similar pattern, i.e. a larger serration event is followed by a succession of additional smaller serration events (see Fig. 7e and f). We can reasonably conceive that the increase in the density of shear bands for the BMG wrapped in an Ni sleeve can tailor the elastic energy stored in one larger serration event (such as the serration events in the original BMG), i.e. the elastic energy is spread more homogeneously over several serration events with smaller amplitude, due to the density of shear bands increasing. This tailoring process pushes the dynamic system, i.e. the serrated flow, to approach the critical state. Thus a significant SOC behavior is achieved and the plasticity is improved. The improvement in the plasticity of the BMG through the electrodeposition of nickel on the sample surface provides solid evidence to support our conjecture, i.e. if shear avalanches in the serrated flow stage can self-organize to a critical state, then the occurrence of fracture can be postponed and BMGs can achieve good ductility.

## 5. Conclusion

In summary, our results explicitly show that the universality of the scale-free intermittent flow can be applied to glassy metals. The power-law distributions for the shear avalanche size for a wide range of plasticities give evidence that serrated flow dynamics is a new example of a self-organized critical system. The relationship between the distribution of shear avalanches and the plasticity of BMGs

suggests that the shear avalanches self-organized to a critical state can help improve ductility. The artificial external disturbance of plastic instability to enhance SOC behavior can effectively improve the ductility of glassy metals, which could be especially important for toughening glassy materials. This newly discovered dynamic critical behavior shows a hitherto unexplored approach for the deformation of glassy metals, which is possibly valid for other glassy systems sharing similar dynamics, including polymers and oxidized glasses at the mesoscopic scale.

## Acknowledgement

The work described in this paper was supported by the Research Committee of Hong Kong Polytechnic University under the project code G-YX90.

## References

- [1] Gilman JJ. Dislocation in solids. Amsterdam: North-Holland; 1983. p. 185.
- [2] Portevin A, Le Chatelier F. CR Acad Sci 1923;176:507.
- [3] Miguel MC, Vespignani A, Zapperi S, Weiss J, Grasso JR. Nature 2001;410:667.
- [4] Richeton T, Weiss J, Louchet F. Nature Mater 2005;4:465.
- [5] Dimiduk DM, Woodard C, Lesar R, Uchic MD. Science 2006;312:1188.
- [6] Csikor FF, Motz C, Weygand D, Zaiser M, Zapperi S. Science 2007;318:251.
- [7] Liu YH, Wang G, Wang RJ, Zhao DQ, Pan MX, Wang WH. Science 2007;315:1385.
- [8] Hofmann DC, Suh J-Y, Wiest A, Duan G, Lind M-L, Demetriou MD, et al. Nature 2008;481:1085.
- [9] Wang WH. J Appl Phys 2006;99:056903.
- [10] Jiang WH, Liu FX, Liaw PK, Choo H. Appl Phys Lett 2007;90:181903.
- [11] Das J, Tang MB, Kim KB, Theissmann R, Baier F, Wang WH, et al. Phys Rev Lett 2005;94:205501.
- [12] Koslowski M, LeSar R, Thomson R. Phys Rev Lett 2004;93:125502.
- [13] Weiss J, Marsan D. Science 2003;299:89.
- [14] Pan XF, Zhang H, Zhang ZF, Stoica M, He G, Eckert J. J Mater Res 2005;20:2632.
- [15] Jensen HJ. Self-organized criticality. Cambridge: Cambridge University Press; 1998. p. 11.
- [16] Birkhoff GD. Proc Natl Acad Sci USA 1931;17:656.
- [17] Malandro DL, Lacks DL. J Chem Phys 1999;110:4593.
- [18] Dyre JC. Rev Mod Phys 2006;78:953.
- [19] Dyre JC, Olsen NB. Phys Rev E 2004;69:042501.
- [20] Argon AS. Acta Metall 1979;27:47.
- [21] Spaepen F. Acta Metall 1977;25:407.
- [22] Falk ML, Langer SJ. Phys Rev E 1998;57:7192.
- [23] Langer JS. Phys Rev E 2004;70:041502.
- [24] Johnson WL, Demetriou MD, Harmon JS, Lind ML, Samwer K. MRS Bull 2007;32:644.
- [25] Lu ZB, Li JG, Shao H, Gleiter H, Ni X. Appl Phys Lett 2009;94:091907.
- [26] Zhang Y, Greer AL. Appl Phys Lett 2006;89:071907.
- [27] Pan D, Inoue A, Sakurai T, Chen MW. Proc Natl Acad Sci USA 2008;105:14769.
- [28] Lewandowski JJ, Greer AL. Natl Mater 2006;5:15.
- [29] Demetriou MD, Harmon JS, Tao M, Duan G, Samwer K, Johnson WL. Phys Rev Lett 2006;97:065502.
- [30] Liu CT, Heatherly L, Easton DS, Carmichael CA, Schneibel JH, Chen CH, et al. Metall Mater Trans A 1998;29:1811.

- [31] Busch R, Kim YJ, Johnson WL. *J Appl Phys* 1995;77:4039.
- [32] Yang B, Morrison ML, Liaw PK, Buchanan RA, Wang GY, Liu CT, et al. *Appl Phys Lett* 2005;86:141904.
- [33] Freltoft T, Kjems JK, Sinha SK. *Phys Rev B* 1986;33:269.
- [34] Bak P, Tang C, Wiesenfeld K. *Phys Rev Lett* 1987;59:381.
- [35] Luque B, Miramontes O, Lacasa L. *Phys Rev Lett* 2008;101:158702.
- [36] Main I. *Geophysics* 1996;34:433.
- [37] Ma D, Stoica AD, Wang X-L. *Natl Mater* 2009;8:30.
- [38] Yu P, Liu YH, Wang G, Bai HY, Wang WH. *J Mater Res* 2007;22:2384.
- [39] Ruud JA, Josell D, Spaepen F, Greer AL. *J Mater Res* 1993;8:112.
- [40] Chen WN, Ravichandran G. *J Mech Phys Solids* 1997;45:1303.
- [41] Zhang Y, Wang WH, Greer AL. *Natl Mater* 2006;5:857.